An Approximate Estimate of the Shear Stress During Roll Forming

D.J. Seo[1], M. D. Martinez[2]

[1]Hansol Research and Development, Daejeon, South Korea, djseo@hansol.co.kr
[2]Dept of Chemical and Biological Engineering, 2260 East Mall, Vancouver BC Canada, martinez@chml.ubc.ca

Introduction

The concept of roll forming simply implies that the sheet is formed through a filtration-type mechanism between two fabrics. Here, dewatering occurs in two distinct steps. In the first step, water and fine material are forced through the wires by the initial momentum of the jet. In the second step, water removal is achieved by the tension and convergence of the fabrics. In both of these steps the change in curvature of the fabrics generates a pressure field to balance the fabrics' tension. Early attempts to characterize the hydrodynamics of twin-wire formers were largely estimates of this pressure

It is clear that the magnitude of the pressure gradient has a significant effect on paper properties. Beyond this, little is known about how the hydrodynamic forces control material distribution and fibre orientation. This raises the questions: (1) what is the magnitude of the hydrodynamic shear required to cause material redistribution; and (2) how much shear is generate on an operating paper machine? It is the latter question of which we address in this work.

In this paper we consider:

1 The two-dimensional flow of fluid with viscosity μ in a curved channel (see Figure 1). The channel is bounded a Newtonian above (i = 1) and below (i= 2) by flexible porous wires of permeability k_i .

2 The position of the upper wire $g(s)$ is unknown *a priori* and the bottom wire follows a trajectory with radius of R. Dewatering occurs through both boundaries over a distance $R\theta$, where θ is the angle of wrap. The domain is bounded by $[r,s]= [R,R + g(s)]\times[0,R\theta]$.

3 The channel has an initial clearance of g_o. The fabrics move at a velocity U_w and the initial velocity of the suspension U_j is known. Motion is induced by drainage through the fabrics and is driven by the momentum of the jet and by the tension T and curvature of the permeable upper fabric.

4 The pressure P (r,s) *is assumed* to be atmospheric initially (P_a) and reaches its equilibrium value of T/R at the end of the domain.

5 The flow field has two viscous boundary layer regions at the upper and lower boundaries. The flow in the central core of the channel is termed the outer flow and can be approximated using potential flow theory.

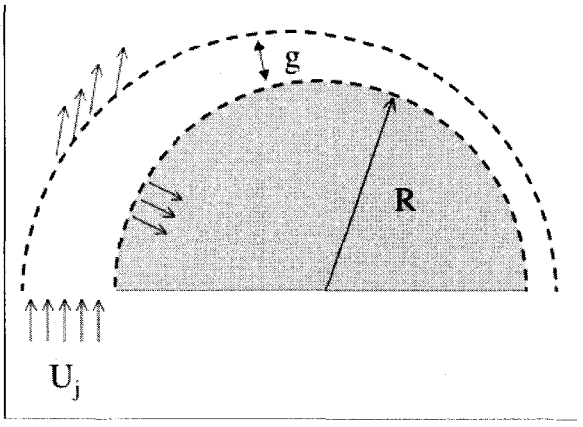

Figure 1: A schematic of the geomtry considered. The hatched lines indicate that the boundary walls are permeable

Model Equations

The model equations for this geometry are those outlined by [Holm & Söderberg (2005a)]. [Holm & Söderberg (2005a)] posed the problem using the Navier-Stokes equation in con-junction with the continuity relationship. In their analysis, they reduced the equations of motion to something more tractable by estimating the order of magnitude of each derivative and eliminating the smaller terms. In their notation, the dominant terms are given by

$$\rho v_\theta \frac{\partial v_\theta}{\partial s} = -\frac{\partial p}{\partial s} + \mu \frac{\partial^2 v_\theta}{\partial s^2} \tag{1}$$

$$\rho \frac{v^2 \theta}{r} = \frac{\partial p}{\partial r} \tag{2}$$

$$\frac{\partial v_\theta}{\partial s} + \frac{\partial v_r}{\partial r} = 0 \tag{3}$$

where v_θ and v_r are the velocities of the fluid in the machine and radial directions, respectively. [Holm & Söderberg (2005a)] did not explicitly discuss *all* the boundary conditions required to solve this system of equations. They did however discuss the force balance on the upper wire required to determine its position, that is

$$P - P_a = T\left(\frac{1}{R} - \frac{d^2 g}{ds^2}\right), \quad r = R + g(x) \tag{4}$$

We compliment the work of [Holm & Söderberg (2005a)] by including the other boundary conditions required to solve the system of equations. Indeed, at the lower boundary $r = R$ we set

$$v_\theta = U_w \tag{5}$$

$$v_r = \frac{P - P_v}{k_2} \tag{6}$$

where k_2 is the drainage resistance of the wire; and P_v is the *absolute pressure* in the roll. These conditions indicate that there is no-slip in the machine direction and that there is drainage or seepage normal to the permeable wire. The drainage or seepage rate is described using Darcy's law. This, too, may be an oversimplification as a higher Reynolds number expression, such as Forcheimer's expression may be more appropriate especially at the point of jet impingement. We invoke Darcy's law for simplicity in order to avoid the inherent non-linearity of the Forcheimer relationship. At the upper boundary, $r = R+g(s)$, we set

$$v_\theta \approx U_w \tag{7}$$

$$v_r = \frac{P - P_a}{k_1} - U_w \frac{dg}{ds} \tag{8}$$

where k_1 is the drainage resistance of the upper wire. Again these equations indicate a no-slip and penetration relationship is invoked at the upper boundary. Equation 7 is written as an approximation. This is done as the boundary condition at this point is a combination of the projections of the wire velocity and seepage velocity in the θ-direction. We have neglected the seepage component as it is small in comparison to the sped of the wire. In Equation 8, the first term on the right hand side of the equation represents drainage through Darcy's law. The second term describes the fact that the permeable wire is moving relative to the flow. At the left and right ends of the domain

$$v_\theta(r,0) \approx U_j, \quad P(r,0) = P_a, \quad P(r,R\theta) = T/R \tag{9}$$

Finally, It must be noted that the conditions at the upstream and downstream locations may not be completely accurate as the physics at these points have yet to be properly described. For example, we impose an upstream velocity profile and an initial gap size at the point of jet impingement. We do so for simplicity.

Even with the simplifications discussed thus far, the equations posed are still formidable. We follow the reasoning given by [Holm & Söderberg (2005a)] and consider that except in the immediate neighborhood near the surfaces of the wires, the velocity distributions deviate only slightly from those in frictionless (potential) flow. This assumption will become apparent after we scale the equations of motion. The transition from potential flow to U_w at the walls takes place over a very thin layer, which we define in this work as the boundary layer. In this manner there are two regions to consider, even if the division between them is not sharp:

1. A very thin layer in the immediate vicinity of the permeable walls in which the velocity gradient

$\partial v_\theta/\partial r$ is very large (boundary layer). In this region the shearing stress $\tau = \mu\partial v_\theta/\partial r$ may assume large values.

2. In the remaining central portion of the domain no such large velocity gradients occur and the influence of the viscosity is unimportant. In this region the flow is frictionless and potential.

In the subsequent sections, we shall obtain solutions in these composite regions and then splice the solutions together to create a composite view of the flow field. As will be discussed subsequently, we encountered numerical difficulties when attempting to solve the problem over the entire domain.

We shall now proceed to discuss the scaling of the governing equations. The difficulty we have in this is that we are unsure of the correct characteristic velocity. For example we can scale the equations using a number of reasonable candidates: U_j, U_w, $U_j - U_w$ or even T/Rk. We therefore take some time at this point rationalizing the choice of this velocity. We begin this argument by re-stating that the hydrodynamic pressure in this system must be of the order $P \sim T/R$. If we choose the radius of the roll R as the length scale, it is clear that the magnitude of the pressure gradient in the machine direction must be given by $\partial p/\partial s \sim T/R^2$.

Upon examination of Equation 1, we reason that the order of magnitude of the advective term $(\rho v_\theta \partial v_\theta/\partial s)$ must be similar to that of the pressure gradient. This argument is based on the fact that in the central portion of the channel the viscous stress is negligible and these are the only two remaining terms in the equation. If we scale the velocity using

$$\frac{v_\theta - U_w}{U^*}$$

where U^* is the (unknown) characteristic velocity, and equate the advective to the pressure term in Equation 1, we see that $U^* = T/\rho U_w^2 R$. For consistency with the notation used in [Holm & Söderberg (2005a)] we define where $U^* = \varepsilon/We$. The parameter $We = \rho U_w^2 g_o/T$ is termed the Weber number and is a dimensionless group introduced by [Holm & Söderberg (2005a)]. The second parameter $\varepsilon = g_0/R$ is the ratio of the gap size to the radius of curvature of the roll. As will be demonstrated shortly, this parameter is much smaller than unity. Finally, we need to define the order of magnitude of the radial velocity v_r. We do so by scaling this velocity component using v_r/V^*, where V^* is the characteristic velocity, and determine its magnitude by equating the order of magnitudes of terms in the continuity relationship, i.e. Equation 3. By doing so we see that

$$V^* = \frac{U_w \varepsilon^2}{We}$$

With our estimates given above, we can now scale the model equations with the certainty that the magnitudes of all terms are unity. If we set

$$U = \frac{v_\theta - U_w}{U^*}, \quad V = \frac{v_r}{V^*}, \quad P = \frac{(p - p_a)}{T/R} \tag{10}$$

$$x = \frac{s}{R}, \quad y = \frac{r - R}{g_0}, \quad G = \frac{g(s)}{g_0} \tag{11}$$

the governing equations become

$$\left(1 + \frac{\varepsilon}{We} U\right)\frac{\partial U}{\partial x} = -\frac{\partial P}{\partial x} + \frac{1}{\varepsilon \,\mathrm{Re}}\frac{\partial^2 U}{\partial y^2} \tag{12}$$

$$\frac{We}{1 + \varepsilon y}\left(1 + \frac{\varepsilon}{We} U\right)^2 = \frac{\partial P}{\partial y} \tag{13}$$

$$\frac{\partial U}{\partial x} + \frac{\partial V}{\partial y} = 0 \tag{14}$$

The boundary conditions now read

$$p(x, G) = 1 - \varepsilon \frac{d^2 G}{dx^2} \tag{15}$$

$$U(x, G) \approx 0 \tag{16}$$

$$V(x, G) = \frac{P(x, G)}{\alpha_1} - \frac{We}{\varepsilon}\frac{dG}{dx} \tag{17}$$

$$U(x, 0) \approx 0 \tag{18}$$

$$V(x, 0) = \frac{P(x, G)}{\alpha_2} + \beta \tag{19}$$

$$G(0) = 1 \tag{20}$$

$$P(0, G) = 0 \tag{21}$$

$$U(0, y) = \frac{We}{\varepsilon}\lambda \tag{22}$$

$$P(\theta, G) = 1 \tag{23}$$

Where

$$\alpha = \frac{kg_0}{\rho V_w R}, \quad \beta = \frac{(P_a - P_v)We}{kU_w \varepsilon^2}, \quad \lambda = \frac{U_j - U_w}{U_w}, \quad \mathrm{Re} = \frac{\rho U_w g_0}{\mu} \tag{24}$$

and θ is the angle of wrap.

Before proceeding onto solving this system of equations it is instructive to examine the order of magnitude of the dimensionless groups and to examine the behaviour of the function G and its derivatives. Both of these points give insight into the form of the mathematical solution and aid in justification of the methods used. To begin, this analysis indicates that there are 7 dimensionless groups which govern the problem, that is, ε, *We*, *Re*, α, β, λ, and θ. It is instructive at this point to estimate the order of magnitude of each of these parameters at typical operating conditions. This is given in Table 1. Of interest here is that $\varepsilon \ll 1$ and the ratio of ε /*We* < 1 is a small. These two points will be used in the numerical solution given in the following sections.

ε	*We*	*Re*	α	β	λ	θ
10^{-2}	10^{-2}	10^{5}	10^{0}	10^{0}	10^{0}	10^{0}

Table 1: Estimates of the order of magnitude of the dimensionless groups

Finally, the scaling of the equations of motion ensured that the sizes of the various terms *U, V, G* and *P* were of order unity. For completeness, we should examine the order of magnitude of the boundary conditions. We start this process by examining Equation 15. It is fruitful to examine the implications of this relationship at the upstream point $x = 0$. Here $P = 0$ which implies that

$$\frac{d^2G}{dx^2} = \frac{1}{\varepsilon} \tag{25}$$

Hence the second derivative at $x = 0$ is very large. At $x = 1$ we use the boundary condition $P = 1$ and show that

$$\frac{d^2G}{dx^2} = 0 \tag{26}$$

Upon examination of Equation 17 we can deduce that $dG/dx \sim \varepsilon$ /*We* - a small number. Hence this function *G* behaves in a very unique manner. These results indicate that the size of the gap is of order of unity, its slope is small over the entire domain, but its second derivative is very large near $x = 0$.

Potential Flow - The Outer Solution

Boundary-layer-type behavior must result from the solution of Equation 12 as $(\varepsilon \mathrm{Re})^{-1} \ll 1$ multiplies the highest derivative. We anticipate a potential flow solution in the central core of the channel and boundary layer behavior near the permeable wires. In this section we solve for both the pressure and gap size distribution under the assumption of frictionless flow. We do so by eliminating the second term on the right-hand side of Equation 28. Even with this assumption the model equations still have four unknowns, the velocity field *U* and *V*, the pressure *P* and the gap size *G*. In this section we will reduce the model equations to one high-order non-linear ordinary differential equation for *G*. This equation will then be solved both numerically and approximately using asymptotic methods.

To begin, we seek a solution of the governing equations by expanding *U, V, P* and *G* using a series of the form

$$\varphi(x, y) = \sum_{n=0}^{\infty} \left(\frac{\varepsilon}{We} \right)^n \varphi_n \tag{27}$$

where φ is a variable representing one of the four unknown in this problem. When terms with order $0(\varepsilon)$ and $0(\varepsilon/We)$ are eliminated, the leading order expressions are

$$\frac{\partial U_0}{\partial x} = -\frac{\partial P_0}{\partial x} \tag{28}$$

$$We = \frac{\partial P_0}{\partial y} \tag{29}$$

$$\frac{\partial U_0}{\partial x} + \frac{\partial V_0}{\partial y} = 0 \tag{30}$$

The higher order terms in this expansion can be determined using standard techniques. At this point in the derivation we define the pressure field. This can be

obtained simply by integrating Equation 29 and evaluating the constant of integration through use of Equation 15, that is

$$P(x,y) = 1 - \varepsilon G_{xx} + We(y - G) \tag{31}$$

The first two terms of this equation indicate the pressure change due to the change in curvature of the fabrics and the third term is the centrifugal pressure. For clarity, the subscript $_o$ has been dropped.

At this point we attempt to express the flow field in terms of G. If the stream function is defined as

$$U_p = \psi_y \quad V_p = -\psi_x$$

where the subscript $_p$ refers to 'potential flow', the pressure can be eliminated from Equations 28 and 29 through cross-differentiation leaving

$$\psi_{xyy} = 0 \tag{32}$$

This equation can be integrated directly, with use of conditions 17, 19, 22, and 31 to give

$$\psi = a_0(x) + y\left(a_1(x) + \frac{We}{\varepsilon}\lambda\right) \tag{33}$$

$$a_0(x) = -\int_0^x \left(\frac{1}{\alpha_2}(1 - WeG - \varepsilon G_{xx}) + \beta\right) dx \tag{34}$$

$$a_1(x) = \int_0^x \frac{1}{G}\left(\varepsilon\left(\frac{1}{\alpha_1} - \frac{1}{\alpha_2}\right)G_{xx} + \frac{We}{\varepsilon}G_x - \frac{We}{\alpha_2}G + \gamma\right) dx \tag{35}$$

$$\gamma = \frac{1}{\alpha_2} - \frac{1}{\alpha_1} + \beta \tag{36}$$

Finally, we can derive an expression for the gap size through substitution of Equations 31 and 33 into 28

$$\varepsilon G G_{xxx} - \varepsilon\left(\frac{1}{\alpha_1} - \frac{1}{\alpha_2}\right)G_{xx} + We\left(G - \frac{1}{\varepsilon}\right)G_x + \frac{We}{\alpha_2}G - \gamma = 0 \tag{37}$$

The boundary conditions for this relationship are as follows

$$G(0) = 1 \tag{38}$$

$$G_{xx}(0) = 1/\varepsilon \tag{39}$$

$$G_{xx}(\theta) = 0 \tag{40}$$

Equations 39 and 40 were obtained through use of Equations 21, 23 and 31. Equation 37 has been solved in two different ways:(a) as a standard boundary value problem using MAPLE (a commercially available symbolic solver) and (b) using a traditional singular perturbation expansion method. The resulting expression is given by

$$G(x) \approx 1 + \frac{\varepsilon}{We}\left(1 - \gamma + e^{-\frac{\sqrt{We}}{\varepsilon}x}\right) \tag{41}$$

From this we can estimate the pressure at the surface of the wire P_w and the suspension velocity U_p

$$P_w = 1 - e^{-\frac{\sqrt{We}}{\varepsilon}x} \tag{42}$$

$$U_p(x) = \frac{We}{\varepsilon}\lambda + \int_0^x \frac{1}{G}\left(\varepsilon\left(\frac{1}{\alpha_1} - \frac{1}{\alpha_2}\right)G_{xx} + \frac{We}{\varepsilon}G_x - \frac{We}{\alpha_2} + \gamma\right) dx \tag{43}$$

The results from the numerical solution and the analytical expression are compared in Figures 2 -5 and good agreement is apparent. What is evident is that there is an entrance region where pressure increases rapidly and then an 'established flow" region where the pressure is essentially constant. In the established flow region, the gap size varies nearly linearly. The length of the entrance region x_b can be estimated from Equation 42. If we define the entrance region as that where the pressure is less than 0.99, we see that

$$x_b = 4.6\frac{\varepsilon}{\sqrt{We}} \tag{44}$$

These results are strikingly similar to the measurements reported by [Gooding, McDonald & Rompre], [Hergert

& Sandford], and [Martinez]. What is different between our results and the previously reported experimental work is the pressure wave reported at the end of the forming zone. We too can generate this waviness if we let the drainage resistance α vary as a function of x.

The error in using the analytical expression is compared to the numerical results, see Figure 5. The error in this shows the relative error in comparison to the numerical result. It is clear that under the industrially relevant conditions, the error in using this expression is at most 5%. Because of this, we recommend the use of the analytical solution to determine the gap size.

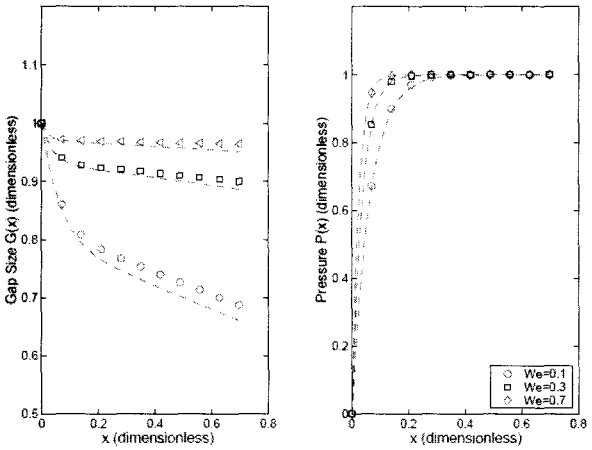

Figure 2: Estimate of the gap and pressure distribution P_w as a function of *We*. The full numerical solution is shown as the symbols and the approximate asymptotic solution as the hatched line. The simulations were conducted with $\varepsilon = 0.02$ and $\gamma = 1$.

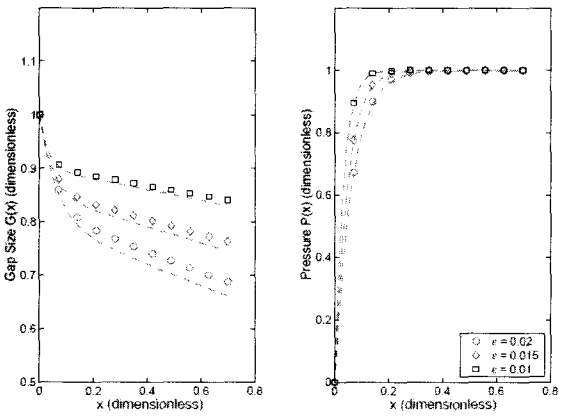

Figure 3: Estimate of the gap and pressure distribution as a function of ε. The full numerical solution is shown as the symbols and the approximate asymptotic solution as the hatched line. The simulations were conducted with *We* = 0.1 and $\gamma = 1$.

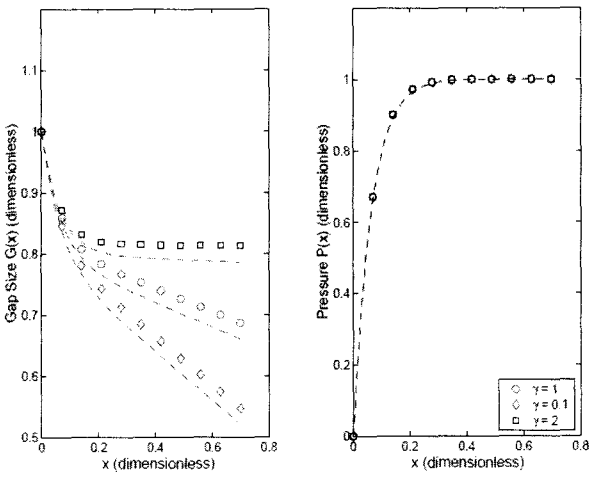

Figure 4: Estimate of the gap and pressure distribution as a function of γ. The full numerical solution is shown as the symbols and the approximate asymptotic solution as the hatched line. The simulations were conducted with *We* = 0.1 and $\varepsilon = 0.02$.

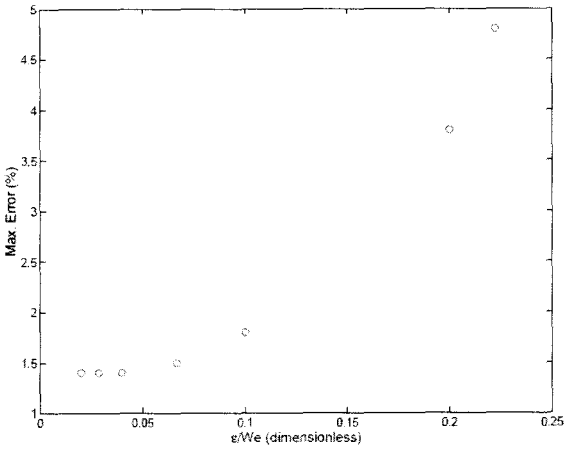

Figure 5: An estimate of the error of the asymptotic expansion with the numerical solution. The comparisons are made with $\gamma = 1$

Estimate of the Viscous Stress

In this section we estimate the viscous stress in the boundary layer through solution of Equation 12. Like most boundary layer type solutions we do so by imposing the pressure field, as given by Equation 31, on the boundary layer regions. We solve this relationship using singular perturbation methods as we can obtain an analytical expression. The analysis will be conducted over both boundary layers : first at $y = 0$ and then at the

upper boundary $y = G(x)$.

We consider the boundary layer near $y = 0$ and seek a solution to Equation 12 using an equation of the form

$$U(x,y;\varepsilon Re) = U_p(x) + w(x,\eta) \tag{45}$$

where $\eta = \sqrt{\varepsilon Re}$. Upon substitution of this in Equation 28 we see that $w(x, \eta)$ must satisfy

$$\frac{\partial w}{\partial x} = \frac{\partial^2 w}{\partial \eta^2} \tag{46}$$

$$w(x,\eta = 0) = -U_p(x) \tag{47}$$

$$w(x,\eta \to \infty) = 0 \tag{48}$$

$$w(0,\eta) = 0 \tag{49}$$

when terms with order less than ε/We have been eliminated. The solution to this is given in standard mathematics text books, such as by [Greenberg], and is

$$w(x,\eta) = -\frac{\eta}{2\sqrt{\pi}} \int_0^x \frac{U_p(\bar{x})}{(x-\bar{x})^{3/2}} e^{-\frac{\eta^2}{x-\bar{x}}} dx \tag{50}$$

In this work, we do not evaluate this expression given above. Instead we solve for the flow field of the simpler problem, Equation 46 using MATLAB's built in solver 'pdepe'. We do this as it is very easy to implement this equation into this solver and the resulting profiles are sensible. The stress τ (having dimensions of P_a) at $\eta = 0$ can be evaluated numerically from this expression

$$\tau = \frac{\mu U_w}{R} \frac{\varepsilon^{3/2}\sqrt{Re}}{We} \frac{\partial w}{\partial \eta} \tag{51}$$

Similarly at y = G(x) we seek a solution of the form

$$U(x,y;\varepsilon Re) = U_p(x) + h(x,\sigma) \tag{52}$$

where $\sigma = (G(x) - y)\varepsilon Re$. Upon substitution of this in Equation 12 we see that $w(x, \eta)$ must satisfy

$$\frac{\partial^2 h}{\partial \sigma^2} = -G_x \frac{\partial h}{\partial \sigma} \tag{53}$$

$$h(x,\sigma = 0) = -U_p(x) \tag{54}$$

$$h(x,\sigma \to \infty) = 0 \tag{55}$$

This gives

$$h(x,\sigma) = -U_p(x) e^{G_x \sigma} \tag{56}$$

It should be noted that this equation is exact when the jet speed equals the machine speed, that is when $\lambda = 0$. If $\lambda \neq 0$ the solution is incorrect in the very small region where $(x, \sigma) \to 0$. This can be corrected for using the method outlined in Appendix A. This analysis shows that the error occurs over a region in space $0 < x < 1/\varepsilon Re$. With this in mind, the stress τ (having dimensions of P_a) at $y = G(x)$ can be evaluated using

$$\tau = \frac{\mu U_w}{R} \frac{\varepsilon^2 Re}{We} G_x U_p \quad x > (\varepsilon Re)^{-1} \tag{57}$$

Estimates of the shear stress acting on the surfaces of the permeable wires are shown in Figure 6. What is evident is that the shear imposed is asymmetric in that the stress on the upper wire is far greater than that on the lower one. This was found for all cases simulated. Further, the stress on the upper wall displays a maximum whose location can be determined by setting the first derivative of Equation 57 equal to zero.

$$x_{max} = \frac{\varepsilon}{2\sqrt{We}} \ln\left(\frac{4\varepsilon^2 We}{\gamma\varepsilon^2 - \varepsilon\sqrt{We} + \lambda We^{3/2}}\right) \tag{58}$$

Finally, the magnitude of the stresses are small yet of the same order of magnitude of the disruptive stress of networks reported by [Raiskinmaki & Kataja]

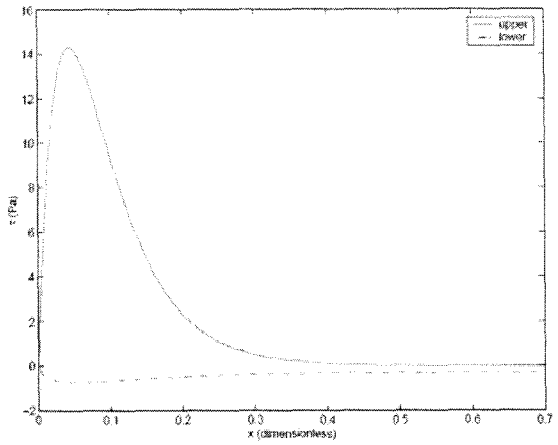

Figure 6: An estimate of the stress acting on the upper and lower boundaries along the length of the machine. This simulation was conducted with $\varepsilon/We = 0.2$, $\alpha_1 = \alpha_2 = 1$, $\beta = 0$, and $U_j = U_w = 1000/60$ m/s.

A Estimate of the Stress in the region (x, σ) → 0

In this region, we expand the function G(x) using a Taylor series approximation as x → 0, i.e.

$$G(x) \approx 1 + \frac{\varepsilon}{We}\left(\frac{\sqrt{We}}{\varepsilon} + \gamma\right)x \tag{59}$$

and seek a solution of the form

$$U(x, y; \varepsilon Re) = U_p(x) + h(x, \sigma) + Q(\xi, \sigma) \tag{60}$$

where $\xi = x\varepsilon Re$. Upon substitution of this in Equation 28 we see that $Q(\xi, \eta)$ must satisfy

$$\frac{\partial Q}{\partial \xi} + G_x(0)\frac{\partial Q}{\partial \sigma} = \frac{\partial^2 Q}{\partial \sigma^2} \tag{61}$$

$$Q(\xi, \sigma = 0) = 0 \tag{62}$$

$$Q(\xi, \sigma \to \infty) = 0 \tag{63}$$

$$Q(0, \sigma) = U_p(0)e^{G_x(0)\sigma} \tag{64}$$

This can be solved using standard techniques.